IEEE Access
Multidisciplinary | Rapid Review | Open Access Journal

Date of publication xxxx 00, 0000, date of current version xxxx 00, 0000.

Digital Object Identifier 10.1109/ACCESS.2017.DOI

MUSIC Spectrum Based Interference Detection, Localization and Interference Arrival Prediction for mmWave IRS-MIMO System

YAFEI HOU[1,2],(Senior Member, IEEE) KAZUTO YANO[1],(Member, IEEE) NORISATO SUGA[1,3],(Member, IEEE) JULIAN WEBBER[1,4],(Senior Member, IEEE) SATOSHI DENNO[2],(Member, IEEE) AND TOSHIKAZU SAKANO[1],(Member, IEEE)

[1]Wave Engineering Laboratories, Advanced Telecommunications Research Institute International, Kyoto, 619-0288, Japan
[2]Faculty of Environmental, Life, Natural Science and Technology, Okayama University, Okayama, 700-8530, Japan
[3]Dept. of Information & Communications Engineering, Shibaura Institute of Technology, Tokyo, 135-8548, Japan
[4]Dept. Electronics & Communications Engineering, Kuwait College of Science and Technology, Doha Area, 7th Ring Road, Kuwait

Corresponding author: Yafei Hou (e-mail: yfhou@okayama-u.ac.jp).

These research results were obtained from the commissioned research (No. JPJ012368C03401) by National Institute of Information and Communications Technology (NICT), Japan.

ABSTRACT For a millimeter wave (mmWave) intelligent re-configurable surface (IRS)-MIMO system, if it can correctly detect the interference occurrence and their locations, the patterns of interference signal can be collected and learned using machine learning for the prediction of interference arrival. With the information of interference location and activity pattern, the capacity of the system can be largely improved using many techniques such as beamforming, interference cancellation, and transmission scheduling. This paper aims to detect interference occurrence using a low-complexity MUSIC (MUSIC: multiple signal classification) spectrum-based method, and then localize their sources for mmWave IRS-MIMO system. The MUSIC spectrum of wireless system can be regarded as somehow the 'signature' related to the signals transmitted from different users or interference. We utilize such property to detect the occurrence of interference, and then localize their sources in a low-complexity way. Finally, the pattern of interference occurrence can be learned to predict the interference arrival from the collected data. This paper also proposed an efficient probabilistic neural network (PNN)-based predictor for the interference arrival prediction and showed its prediction accuracy. From simulated results, our proposed method can achieve the correct results with the accuracy near to 100% when the fingerprint samples is over 10. In addition, the localization error can be within 1 m with more than 65% and 43% for Y-axis and X-axis, respectively. Finally, based on the results of the interference occurrence, the proposed PNN-based predictor for the interference arrival prediction can capture correctly the similar distribution function of the coming continuous idle status.

INDEX TERMS Interference detection, MUSIC spectrum, Interference localization, Prediction of interference arrival, Probabilistic neural network.

I. INTRODUCTION

For the coming B5G era, wireless system is aiming to be more sophisticated with diverse applications like virtual reality, augmented reality, remote monitoring, telemedicine and remote healthcare which require ultra-high-speed, high-capacity communication [1]. The amount of wireless traffic will continue to increase explosively. It is challenging to achieve the highly reliable and large-capacity wireless communication and to provide the sufficient wireless infrastructure for applications in the B5G era. To realize such targets for the coming B5G and 6G era, wireless system needs to not only utilize new high-frequency bands with unused large bandwidth for ultra-high-speed wireless system, but also develop technology to suppress interference that occurs between different wireless systems over the same frequency band [2]. In addition, to accommodate massive devices, it is

necessary to further reduce the traffic density by reducing the distance between wireless devices or the spatial separation among wireless cells [3]. In such high-density environment, the interference among different systems is more severe which needs for more sophisticated technology to reduce interference for the private communication systems such as wireless LAN and radar systems, etc [4].

In response to this, recently, a powerful and novel low-cost intelligent re-configurable surface (IRS) is becoming one of hot and important research topics. Massive unit cells are designed and integrated into IRS devices without or with several radio frequency (RF) chains. Each designed cell can control the reflected waves to the appropriate directions according to the different design targets. This novel device is promising to be employed to configure some cognitive/smart radio environments for the different purposes of wireless systems [5]. IRS devices can be utilized for many scenarios such as at building, wall/ceil of room, building, shopping mall, vehicular, etc. Due to these merits, in recent years, many interesting research topics and projects related to the usage of IRS appeared, especially over Millimeter (mm) wave band where one IRS can hold more cells. IRS is attracting worldwide attention as one of the technological elements that will be utilized for B5G system.

To share the same frequency band with other systems and transmit data with sufficient communication quality to as many users as possible, mmWave MIMO (multiple-input and multiple-output) technique is employed as one major technology for B5G wireless systems [6]. MmWave MIMO systems can hold massive antennas as an antenna array because of its short wavelength, which significantly enhances the system capacity, and supports more accesses from users [7]. In addition, the vast frequency resource over mmWave band (30∼300 GHz) can be utilized to achieve over 100 times capacity than that of current wireless system [8]. Such high capacity further excites novel wireless applications for B5G/6G era, including V2V/V2I communication, wireless high definition television, medicare etc [9]. Therefore, many researches aim to utilize IRS technologies to further improve the spectral efficiency or capacity of mmWave system.

One important topic for mmWave system is to mitigate or reduce the cochannel interference (CCI) generated from the undesired users. It is assisted by two technologies: the interference detection and the prediction of interference arrival. The purpose of interference detection [10] is to correctly judge whether the collected signal is mixed with the signal transmitted from some undesired users and then estimate their directions or locations correctly if interference occurs. The interference arrival prediction tries to predict the timing of the interference occurrence, interference duration, its transmission pattern based on the collected data and information [11]. The correct interference detection is essential to find the correct pattern of interference arrival. Without correct detection, the collected data and information on interference arrival is totally mismatched with the real case which results in the wrong prediction results. These ongoing researches are important for the next generation mmWave wireless system. If the correct directions or locations of these interference sources are correctly captured, some smart beamforming control techniques can alleviate or suppress the interfering signals by change the nulls of the beamforming to face to the directions of these interference signal. For a mmWave massive MIMO system combined with an IRS device, the more accurate localization the transmitter can obtain, the higher capacity the whole wireless system can achieve. In addition, if it knows the start, end of interference duration and transmission pattern of the interference sources, the transmitter can avoid its useless transmission and save the energy by rescheduling its beamforming patterns.

Many researches have focused on the interference detection for different systems [12]. Some researches have proposed a time-frequency signal detection method for a microwave oven (MWO) system [13, 14] to achieve reliable wireless communication with the experimental signal data captured in a shielded room. They showed that the proposed methods can correctly detect the interference signal of inverter MWO. In addition, the proposed method is robust against many products, environments, and different signals. The authors in [12] have proposed a lightweight method for identifying the interference using the data of the model-aided spectral features and the real-time extraction of envelope from the IEEE 802.15.4, 802.11b/g/n, 802.15.1, and Bluetooth Low Energy (BLE) wireless systems. Some researches focus attentions on the coexistence between the radar systems and IEEE 802.11 WLAN systems in adjacent or coherent channel scenarios. The authors in [15] have designed one modified receiver. This new receiver includes a log-likelihood ratio mapping function and a new inter-leaver layer to suppress the interference from the radar systems. Our early work has proposed a methodology for classifying the interference type to improve the accuracy of wireless throughput prediction using the received signal strength indicator (RSSI) data collected from both the measurement campaign and simulation [16]. With multiple time-frequency scalogram images calculated from the collected data, the interference classification and spectral features can be classified correctly on over 65% of the occasions when using the convolutional neural network.

In addition, for the localization of users over indoor scenarios, there also exists many research results [17]. Most of the radio-based localization methods in wireless communication measure the received signal strength indicator (RSSI), angle of arrival (AOA), time of arrival (TOA), and time difference of arrival (TDOA), and then convert these signal characteristic information into target location. To improve localization accuracy, some fingerprinting-based systems are adopted to mitigate the negative effects of multi-path propagation [18]. Many machine learning (ML)-based localization schemes such as K nearest neighbors (KNN), support vector machine (SVM), and artificial neural network (ANN) have been proposed in the past years [19]. Recent advanced IRS technology also stimulates the usage of IRS and signal

process on the user localization. The reference [20] has provided a systematic overview of existing researches on IRS usage from the signal processing point of view, which focusing on channel estimation, transmission design and radio localization. In addition, for IRS usage on localization over mmWave or high-frequency terahertz (THz) band, the reference [21] has proposed a near-field channel estimation and localization algorithm based on the derived second-order Fresnel approximation of the near-field channel model. These methods provided some trade-off results between the localization accuracy and computational complexity.

In this paper, we will propose a MUSIC (multiple signal Classification) [22] spectrum-based method to detect the occurrence of interference, and then localize its interference source for a mmWave IRS-MIMO wireless system. After that, the pattern of interference occurrence is learned from the collected data to learn and predict the interference arrival. This paper also shows the prediction accuracy when it utilizes a probabilistic neural network (PNN) for prediction. Compared with the other MUSIC spectrum based methods for mmWave MIMO system, our research utilizes the MUSIC spectrum calculated from the mmWave IRS-MIMO channel. Due to IRS usage, the distribution of multipaths and link amplitudes between the transmitter and receiver will be changed, which largely impacts the MUSIC spectrum and makes the results of occurrence detection and localization be different compared with that of mmWave MIMO system. The novelties and major contributions are listed as follows.

1) Usually, for a mmWave IRS-MIMO system with multiple antennas set with a uniform linear array (ULA), the auto-correlation operation process on the ULA signal can benefit the estimation of the arrival of angles (AoAs) of all signals transmitted from different users [24]. The MUSIC method can estimate the noise subspace from the available auto-correlation vectors and search the user related steering vectors that are orthogonal to the noise subspace. Usually, the AoAs are expressed by the peaks values of the MUSIC spectrum. Therefore, the MUSIC spectrum can be regarded as a kind of 'signature' related to the signals transmitted from different users at different locations. In this paper, we will utilize this property to detect the interference occurrence in a low-complexity way.
2) Since the signals transmitted from different locations can generate different MUSIC spectrums, in a similar way, the MUSIC spectrum can also be used for fingerprint-based localization. This paper also proposes a low-complexity MUSIC spectrum-based localization method to estimate the interference locations correctly considering two different IRS patterns.
3) After obtaining the data related to the pattern of interference occurrence, it is possible to utilize the time-series data to learn the correlation and predict the probability of interference arrivals. In this paper, we also propose a prediction method for estimating the probability of interference arrival using a PNN-based predictor.

This paper is organized as follows. In Section II, we describe the used channel model of mmWave IRS-MIMO system. In Section III, the proposed MUSIC spectrum-based interference detection and localization method are explained. Then the simulated results of the proposed interference detection and localization are shown in Section IV. The PNN-based predictor for interference arrival and its prediction performance are discussed in Section V. In Section VI, the paper concludes the main results and some issues.

II. THE CHANNEL MODEL OF MMWAVE IRS-MIMO COMMUNICATION SYSTEM

The uplink channel model with multiple users of a mmWave IRS-MIMO wireless system which we used in this paper is shown in Fig. 1. We assume there are N_U user equipment (UEs) with L antennas each and one base station (BS) with K antennas, respectively. The system has one IRS device which includes M cells and the ith cell can control or adjust its phase of radio wave as $\omega_{i,t}$ at the time t. Therefore, the IRS pattern can be represented using an $M \times M$ size matrix $\mathbf{\Omega}_t$ with the diagonal values as $[\omega_{1,t}, ...\omega_{M,t}]$.

We define the center of IRS to be the origin of 3-D space (0,0,0), and utilize P_m to represent the 3D location (x_m, y_m, z_m) of the mth UE. For mmWave wireless system used for indoor scenarios, usually, the near-field wireless channel model [25, 26] is represented using a spherical wave model with three parameters (d_m, ϑ_m, φ_m) as shown in the right side of Fig. 1. Here the distance between the center of IRS and the mth UE is represented with d_m. The AoAs $\varphi_m \in [0, 2\pi]$ and $\vartheta_m \in [0, \pi/2]$ are the angle between the X-axis and the projection of P_m on the X-Y plane, and the angle between input wave and the Z-axis, respectively.

Therefore, a wave-vector function $\kappa(\vartheta_m, \varphi_m)$ with parameters ϑ_m and φ_m can be shown as

$$\kappa(\vartheta_m, \varphi_m) = -\frac{2\pi}{\lambda} \begin{bmatrix} \sin\vartheta_m \cos\varphi_m \\ \sin\vartheta_m \sin\varphi_m \\ \cos\vartheta_m \end{bmatrix}. \quad (1)$$

$\kappa(\vartheta_m, \varphi_m)$ can be used to calculate the position of the UE as $\mathbf{p}_m = -\lambda d_m \kappa(\vartheta_m, \varphi_m)/2\pi$ with $d_m = \|\mathbf{p}_m\|$.

The received wireless signal $y_{km}(t)$ at the kth receiver antenna of BS over the channel from the mth UE with symbols $s_{ml}(t)$ at the lth transmitter antenna ($l = 1, ..., L$) can be represented as

$$y_{km}(t) = \sum_{l=1}^{L} \left\{ e^{j\theta_{kml}} (\rho(P_k) \circ e^{j\alpha(P_k)})^T \mathbf{\Omega}_t (\rho(P_{ml}) \circ e^{j\alpha(P_{ml})})(t) + h^{kml}_{UEBSLOS}(t) + \sum_{a=1}^{N_{lm}} h^{kma}_{UEBSNLOS}(t) \right\} s_{ml}(t). \quad (2)$$

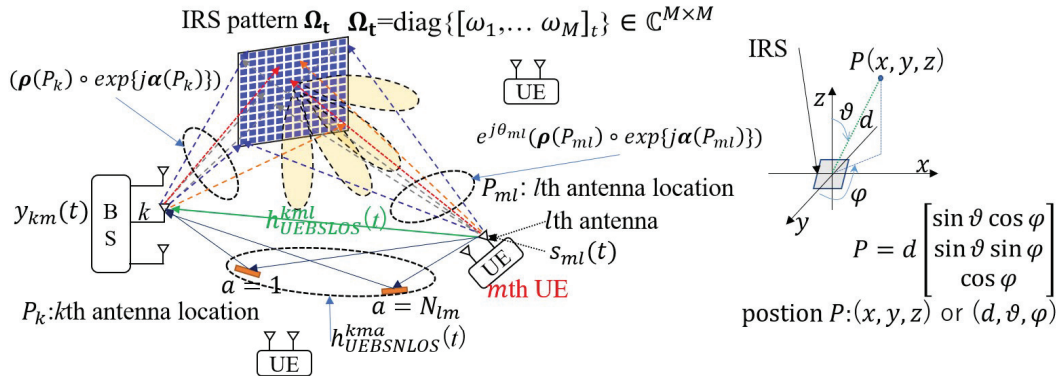

FIGURE 1. The channel model of IRS-MIMO wireless uplink system.

Here $e^{j\theta_{kml}}$ shows the phase offset generated from the imperfect system mismatch and operation between the lth transmit antenna of the mth UE and the kth receive antenna. Usually, the phase offset can be assumed as 0. We use the operator $\circ$ here as the point-wise product of two same size vectors. $\rho(P_{ml}) \in \mathbb{R}^{M\times 1}$ and $\alpha(P_{ml}) \in \mathbb{R}^{M\times 1}$ are the amplitude and phase values of the wireless path among the IRS elements and the lth transmit antenna of the mth UE. The value of $\rho(P_{ml})$ and $\alpha(P_{ml})$ are calculated using the value of distance and wavelength and path loss model. Therefore, the complexity-value vector $\rho(P_{ml}) \circ e^{j\alpha(P_{ml})} \in \mathbb{C}^{M\times 1}$ is the wireless channels between the lth transmit antenna of the mth UE and the IRS elements. In a similar way, the parameters $\rho(P_k) \circ e^{j\alpha(P_k)}$ represent the amplitude and phase values of wireless path between the IRS elements and the kth receive antenna of BS. The superscripts $[.]^T$ used here represents the transpose value of its argument. Therefore, the value as $\rho(P_k) \circ e^{j\alpha(P_k)})^T \mathbf{\Omega}_t (\rho(P_{ml}) \circ e^{j\alpha(P_{ml})}$ can be treated as the channel link between the lth transmit antenna of the mth UE via IRS device and the kth receive antenna.

We use $h^{kml}_{UEBSLOS}$, and $h^{kma}_{UEBSNLOS}$ to represent the LOS part and the ath reflected wave of NLOS part with N_{km} reflected multiple paths between the kth receive antenna and the mth UE.

With Eq. (2), the received symbol $y_k(t)$ at the kth receive antenna of BS from N_U UEs can be represented as

$$y_k(t) = \sum_{m=1}^{N_U} y_{km}(t) + n_k(t) \tag{3}$$

where $n_k(t)$ is the additive Gaussian noise (AWGN) with its variance as $N_0/2$ at the kth receive antenna.

The channel model used for the link between one IRS device and the receive/transmit side such as $\rho(P_k) \circ \alpha(P_k)$ is classified with two types. When the distance between the IRS device and receive/transmit is larger than Rayleigh distance $2D^2/\lambda$ (D: radiation aperture of IRS) which called as far-field (Fraunhofer region), the channel model is usually treated as the plane-wave model. On the other hand, if the distance is smaller than $2D^2/\lambda$, the near-field spherical-wave model is usually used for representing the channel model. The channel model of IRS device [25, 26] considering for the far-field case can be represented as

$$\rho(P) = \rho \mathbf{1}_M, \quad [\alpha(P)]_i = \exp(-j\mathbf{q}_i^T \kappa(\vartheta,\varphi)) \tag{4}$$

where $\rho^2 = f(\vartheta,\varphi)\frac{A\cos\vartheta}{4\pi d^2}$, $\mathbf{q}_i$ is the 3D location of the ith IRS cell center. Here parameter A is represented as the size or area of IRS element. $f(\vartheta,\varphi)$ is a correction factor for the adjustment of the signal input power as $1-\sin^2(\vartheta)\sin^2(\varphi)$. This equation also shows that for the far-field channel model, the distance between the antenna and center point of each IRS element has no impact on the phase value.

For other indoor cases, channel models for the mmWave system with short wavelengths are usually assumed as the near-field one. For the near-field case, the channel model between the mth UE and the IRS device can be calculated as

$$\rho(P) = \rho \mathbf{1}_M, \quad [\alpha(P)]_i = \exp(-j\frac{2\pi}{\lambda}(||P_m - \mathbf{q}_i|| - d_m)). \tag{5}$$

Due to the short distance and wavelength, the distance between the location of UE (P_m) and the center point of each IRS element can largely change the phase value. In addition, When $d_m \gg \mathbf{q}_i, \forall i$, the near-field channel model will revert to that of the far-field one. Usually, the channel model is related to the transmission distance. If the wireless system is assumed to be operated over 60 GHz with a scenario like a small indoor office. From Rayleigh distance and Fraunhofer condition [27] , the channel model can be treated as near-field one.

It should be noted that, in Eqs. (4) and (5), the power loss model is related with d^{-2}. The different power loss model for different frequency band can also be used in our proposed method.

III. THE PROPOSED INTERFERENCE DETECTION AND LOCALIZATION USING MUSIC SPECTRUM

To find the accurate interference status and their locations, it is necessary to correctly estimate much information on the transmit and the interference sources such as their AoAs, received powers, channel models etc. Generally, it is impossible to realize such target due to the limitation of computational complexity (CC) and the execution time [28, 29]. For

some application scenarios, the requirement of interference detection level and localization accuracy are different. The higher accuracy of interference detection is better. However, for the localization accuracy, it is enough if the estimation error can be achieved within 1 m or 2 m for some location-aware applications. This eased requirement largely reduces the difficulty of realization for the real-time usage of the proposed MUSIC spectrum-based interference detection and localization.

Many MUSIC spectrum-based AoA estimation methods have been investigated and proposed especially for the channel model with far-field case. In these scenarios, the plane-wave model is utilized for algorithm design in an easy and simple way. Among them, one popular and important method is the MUSIC method [30] which employs the SVD decomposition on the autocorrelation matrix calculated from the received signal to find its eigenvectors and eigenvalues. Then by searching and calculating the steering vectors which are almost orthogonal to the noise subspace, the AoAs information can be estimated using these steering vectors. Generally, these important steering vectors are also called as MUSIC spectrum.

From Eqs. (2) and (3), one simplified equation can be used to show the received signal at the kth antenna related to the AoAs (ϑ_m, φ_m) from the mth UE as follows

$$y_k(t) = \sum_{l=1}^{L} f_m^l(\vartheta_m, \varphi_m) s_l(t) + n_k(t). \tag{6}$$

It should be noted that the above equation only includes a single UE. It is easy to change the equation for considering the case with multiple UEs.

Let us suppose the received signal at all K receive antennas to be represented as

$$\mathbf{y}_t = \mathbf{A}\mathbf{s}_t + \mathbf{n}_t. \tag{7}$$

Here $\mathbf{A}$ is $[\eta(\vartheta_1, \varphi_1), ..., \eta(\vartheta_L, \varphi_L)]$ and $\eta(\vartheta_k, \varphi_k) = [f_k^1(\vartheta_k, \varphi_k), ..., f_k^K(\vartheta_k, \varphi_k)]^T$. $\mathbf{s}_t$ is $[s_1(t), ..., s_L(t)]^T$ and $\mathbf{n}_t$ is $[n_1(t), ..., n_K(t)]^T$. Therefore, the auto-correlation operation on the received signal $\mathbf{y}_t$ can be shown as

$$\Re_{yy} = \mathbb{E}\{\mathbf{y}_t \mathbf{y}_t^H\} = \mathbf{A}\mathbb{E}\{\mathbf{s}_t \mathbf{s}_t^H\}\mathbf{A}^H + \sigma_n^2 \mathbf{I}. \tag{8}$$

Here $\mathbb{E}$ and superscript $[.]^H$ represent the average operator and the conjugate transpose, respectively.

The MUSIC spectrum can be obtained with the eigenvalue decomposition operation on the K-by-K matrix $\Re_{yy}$. We assume that $\mathbf{s}_t \mathbf{s}_t^H$ is a matrix as $\mathbf{I}$ with unit power, then the Eq. (8) can be decomposed as

$$\Re_{yy}\mathbf{e}_i = [\mathbf{A}\mathbb{E}\{\mathbf{s}_t \mathbf{s}_t^H\}\mathbf{A}^H + \sigma_n^2 \mathbf{I}]\mathbf{e}_i = (\mu_i + \sigma_n^2)\mathbf{e}_i = \lambda_i \mathbf{e}_i, \tag{9}$$

where $\mathbf{e}_i$ and λ_i are eigenvector and its corresponding eigenvalue of $\Re_{yy}$. In addition, these eigenvalues λ_i have following property as

$$\lambda_1 \geq \lambda_2 \geq \ldots \geq \lambda_L \geq \lambda_{L+1} = \cdots = \lambda_K = \sigma_n^2. \tag{10}$$

These $(K - L)$ eigenvectors as the set with $\mathbf{e}_{L+1}, \cdots, \mathbf{e}_K$ which related to the eigenvalues $\lambda_{L+1}, \cdots, \lambda_K$ with values as the noise power σ_n^2 can be utilized for calculating the noise subspace from $\Re_{yy}$.

AoA estimation algorithm usually search the MUSIC spectrum $P(\vartheta, \varphi)$ to find the angle area where is almost orthogonal to the noise subspace. Here the MUSIC spectrum $P(\vartheta, \varphi)$ can be represented with the following equation as

$$P(\vartheta, \varphi) = \frac{\eta(\vartheta, \varphi)\eta^H(\vartheta, \varphi)}{\eta(\vartheta, \varphi)\mathbf{E}_N \mathbf{E}_N^H \eta^H(\vartheta, \varphi)}, \tag{11}$$

where $\mathbf{E}_N = [\mathbf{e}_{L+1}, \cdots, \mathbf{e}_K]$. The MUSIC-based AoA estimation algorithm searches all possible angles to find the L peak values over $P(\vartheta, \varphi)$ by testing all possible combinations of (ϑ, φ). This calculation process has a large increase on the computational complexity (CC) especially when considering the AoA estimation of multiple UEs and channel model with many reflected waves over the near-field spherical wave space.

Using MUSIC spectrum to estimate AoAs has been largely employed for the far-field case, because most wireless waves of channel are treated as plane wave model with only unknown AoAs ϑ. Therefore, the CC of estimation algorithm is reduced for searching ϑ only. In addition, to estimate all possible AoAs, the MUSIC spectrum needs to hold more peak values related to their eigenvectors. This requirement leads to increase value of K, the number of BS antenna of ULA. Furthermore, due to the reflected waves from scatterers and the IRS device, the MUSIC spectrum related to AoAs at the receiver side appears to have complicated properties with an unrecognizable distribution. Therefore, finding the accurate AoAs extremely over a mmWave channel is difficult.

However, it is not necessary to extremely estimate the correct AoAs of all UEs from the MUSIC spectrum. Since MUSIC spectrum could be regarded as the 'signature' related to all the signal transmitted from different users at different locations, it can be processed and utilized as one indicator parameter to show whether the interference signal or interference occurrence appears or not. In addition, by collecting the MUSIC spectrum with interference signal as a fingerprint (FP) of some specific pre-decided locations where the interference source is located, the new calculated MUSIC spectrum, when new interference occurs, can be utilized to localize the unknown interference source coarsely. Based on this idea, we proposed the low-complexity MUSIC spectrum-based method for the interference detection and localization.

The proposed interference detection includes two stages. Firstly, when no interference occurs, one MUSIC spectrum is generated as one fingerprint sample. Since the known UEs usually is not moving or moving with a low speed, these fingerprint samples or MUSIC spectrums have high correlation. The minimum correlation value among these MUSIC spectrums ρ_{Thes} can be used as the threshold or indicator to decide whether the interference occurs or not. Let us assume there are N_S fingerprint samples as $P_{FP}^i(\vartheta), (i = 1, ..., N_S)$. In the next stage of the interference detection, BS only

calculate the correlation values between the new MUSIC spectrum $P_{new}(\vartheta)$ and N_S fingerprint samples $P^i_{FP}(\vartheta), (i = 1, ..., N_S)$. Using the following criterion, the indicator of interference occurrence can be easily judged,

$$\exists i \in [1, ..., N_S], Cor(P_{new}(\vartheta), P^i_{FP}(\vartheta)) \geq \rho_{Thes} \Rightarrow \text{No interference occurs} \quad (12)$$

$$\forall i \in [1, ..., N_S], Cor(P_{new}(\vartheta), P^i_{FP}(\vartheta)) < \rho_{Thes} \Rightarrow \text{Interference occurs} \quad (13)$$

In a similar way, using MUSIC spectrum as fingerprint, we can localize the interference source coarsely when interference occurs. Firstly, the BS divides the whole room space into several small grids and select their centers as known locations where interference source is assumed to be located. Then it builds these known MUSIC spectrums with the interference source located to these selected centers as fingerprint samples. For the stage of localizing the interference source which is randomly located whole room space, if the BS judges that interference occurs, it calculates the correlation degree between the new MUSIC spectrum and these known MUSIC spectrums, and finds the maximum correlation value. Then the location of the random-located interference source is decided as the center position of the grid with this maximum correlation value.

It is easy to understand that the proposed method only localizes the interference source coarsely and the accuracy depends on the size of grids. However, for conventional interference detection and localization, it usually needs to capture the channel status information (CSI) or AoAs correctly which requires more time and computational resources. Our proposed MUSIC spectrum-based method only uses the received signal, and does not calculate any CSI, AoAs between the UEs, BS and IRS devices. Therefore, the proposed method can largely reduce the resource requirement of channel estimation and the computational complexity. It is sure that the proposed localization method has limited localization accuracy. However, such accuracy performance can be further improved using the technique of distributed BSs cooperation, adjustable IRS pattern and machine learning.

IV. SIMULATION RESULTS OF PROPOSED INTERFERENCE DETECTION AND LOCALIZATION

A. SIMULATED SCENARIO AND PARAMETERS

This section shows the simulated performance of the proposed MUSIC spectrum-based method for interference detection and localization. Fig. 2 provides the simulated scenario. We assume that two UEs and one BS are set at (10 m, 5 m, 1.2 m), (5 m, 10 m, 1.2 m) and (0, 5 m, 2 m), respectively. IRS is set at X-axis and its origin points is located at (5 m, 0, 2 m). The reflected surface of IRS faces to the Y-axis direction.

For the IRS pattern $\mathbf{\Omega}_t$, two different cases have been simulated. The first pattern ($\mathbf{\Omega}_t^{IRS\rightarrow BS}$) is set to make the link power between the BS antennas and IRS cells as maximum as possible. This can be realized by separating the

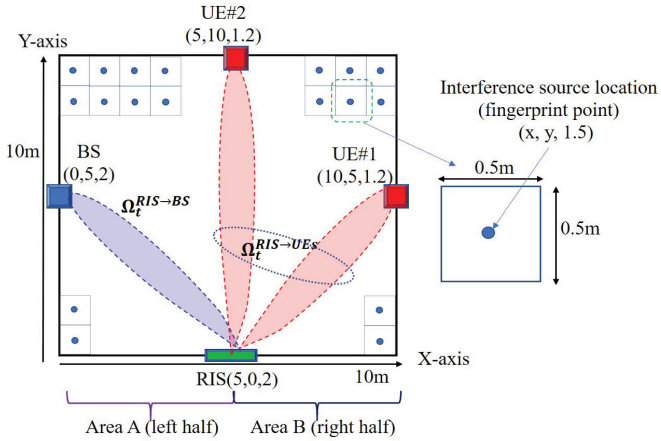

FIGURE 2. The simulated indoor scenario.

IRS cells into several non-overlapped groups according to the number of BS antennas. Then the cells of each group design their reflected phases equal to the conjugate value of channel between the corresponding BS antenna and these cells [25]. In a similar way, the second pattern ($\mathbf{\Omega}_t^{IRS\rightarrow UEs}$) is adjusted to make the value of link power between the UE and IRS cells as maximum as possible.

Table 1 lists the major parameters of the simulated system. We assume the signal of interference and BS-UEs is generated using OFDM symbols and the IFFT size of the system is 2048. The data is transmitted with 1200 subcarriers. The bandwidth is 30.72 MHz which means that one millisecond can hold 14 OFDM symbols similar to the 3GPP standards [31]. The MUSIC spectrum is calculated using one OFDM symbol. In addition, the path loss model is given as followings for indoor scenarios [32].

$$PL = 32.4 + 20\log_{10}(f_c) + 17.3\log_{10}(d) \quad [dB], \quad (14)$$

where f_c is center frequency of wireless system with unit as [GHz]. The IRS channel is generated with the near-field model. The NLOS paths and LOS path are generated using a Ray-tracing model which calculates phase value and the power using link distance between transmit and receive with the path loss model as Eq. (14). The locations of scatterers, which used for calculating the reflected waves for NLOS paths, are generated randomly within the simulated indoor room.

The simulation decides whether the interference occurs or not randomly and runs 4000 times. For each time, if interference occurs, the interference signal is transmitted by an 1.5m-height interference source and its location is randomly generated from [0 m, 10 m] of both Y-axis and X-axis as shown in Fig. 2. Otherwise, the received signal at BS side only includes the signal transmitted from two UEs with the fixed locations as shown in Fig. 2. In addition, the whole indoor space is divided into Area A (left half) and Area B (right half) to compare the influence from the

distance between BS and UEs on the accuracy of interference detection and localization.

TABLE 1. Specifications of simulation

Size of simulation room	X:10 m, Y:10 m, Z(height):5 m
Number of antenna: BS (K) /UE (L)	16 / 4 for two UEs
Spacing among antennas	$\lambda/2$
Number of antenna: interference	1
Center frequency, bandwidth	60 GHz, 30.72 MHz
IRS cells (M), cell spacing	50×50, $\lambda/2$
Transmit power of interference, UE	20 dBm
Used subcarriers /spacing, IFFT size	1200/15 kHz, 2048
Number of scatterers	30
OFDM symbols per 1 ms	14

B. THE SIMULATED PERFORMANCES OF INTERFERENCE DETECTION

Before evaluating the accuracy of interference detection, we need to decide the threshold value of minimum correlation value ρ_{Thes}. This is achieved based on the minimum correlation value of 100 times trial fingerprint samples. After trial test, the threshold ρ_{Thes} are selected as 0.997 for the first case with IRS pattern ($\mathbf{\Omega}_t^{IRS\to BS}$), and as 0.994 for the second case with IRS pattern ($\mathbf{\Omega}_t^{IRS\to UEs}$), respectively.

The results of the interference detection accuracy are shown in Fig. 3 for the first case with IRS pattern as $\mathbf{\Omega}_t^{IRS\to BS}$, and in Fig. 4 for the second case with IRS pattern as $\mathbf{\Omega}_t^{IRS\to UEs}$, respectively. From the results of both figures, when no interference occurs, the proposed MUSIC spectrum-based method can judge the correct results with the accuracy near to 100% when the FP samples N_S is increased to 10. The reason is that large FP samples increase the similarity of among the MUSIC spectrums when no interference occurs. On the other hand, if interference occurs, the detection accuracy is reduced lightly when N_S is increased to 10. It implies that more conditions are necessary in the Eq. (13) to correctly decide the interference occurrence. In addition, when the locations of interference sources are from Area B, the detection accuracy is little degraded due to the high link power loss between BS and the interference source. In both figures, our proposed method can correctly detect the interference occurrence more than 98%.

C. THE SIMULATED RESULTS OF PROPOSED LOCALIZATION METHOD

As shown in Fig. 2, to localize the interference source, we first divided the 2D X-Y plane into 400 grids, and the size of each grid is 0.25 m × 0.25 m. For each grid, as reference for fingerprint sample, the interference source is assumed to be located in the center of the grid. Therefore, 400 kinds of known MUSIC spectrums as fingerprint samples are generated at the BS side in advance. For the stage of localization, BS firstly calculated the new MUSIC spectrum and detected that the interference occurs with the method of previous subsection. Then, the location of interference source is decided as the position of the grid center which

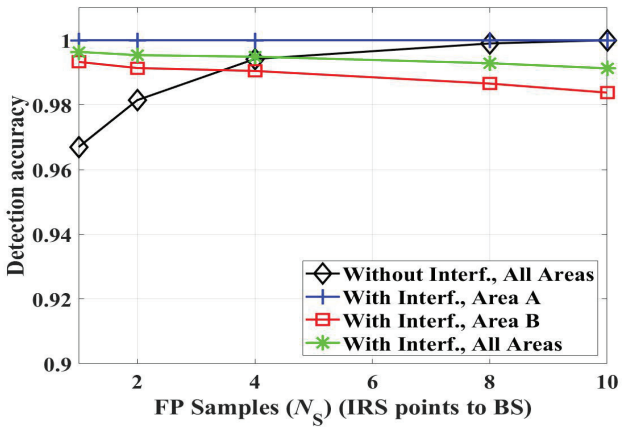

FIGURE 3. The accuracy performance of interference detection (IRS pattern: $\mathbf{\Omega}_t^{IRS\to BS}$) .

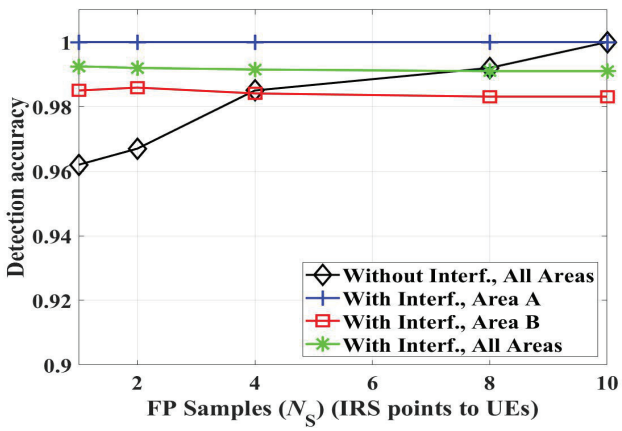

FIGURE 4. The accuracy performance of interference detection (IRS pattern: $\mathbf{\Omega}_t^{IRS\to UEs}$).

has the maximum correlation level among the 400 kinds of known MUSIC spectrums and new MUSIC spectrum. Since the interference sources are randomly generated from the X-Y plane, the localization accuracy is largely decided by the size of grid. Therefore the proposed method only coarsely localizes the interference source.

We use the CDF (cumulative distribution function) of the normalized localization error calculated as ($|X_{true} - X_{estimate}|$) to show the localization performance. The results of location accuracy in X-axis and Y-axis are given in Fig. 5 and Fig. 6 when the IRS patterns are $\mathbf{\Omega}_t^{IRS\to BS}$ and $\mathbf{\Omega}_t^{IRS\to UEs}$, respectively. The results in both figures show the proposed MUSIC spectrum-based localization can coarsely localize the source when interference occurs. For both cases with different IRS patterns, the localization error can be within 1 m with more than 65% and 43% for Y-axis and X-axis, respectively. If the interference source is located in Area A, the probability will be larger for that the error is within 1 m. In addition, as shown in both figures, the

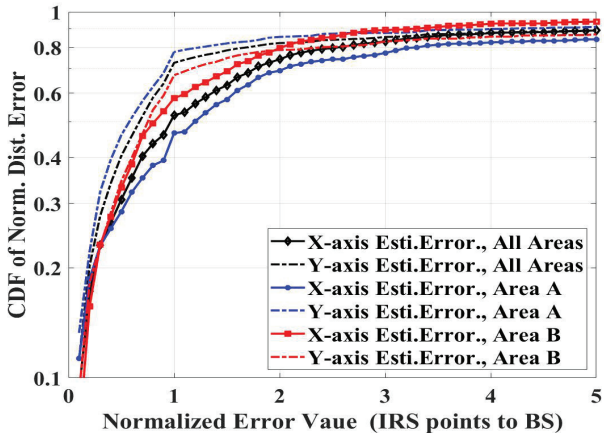

FIGURE 5. The localization performance of interference source (IRS pattern: $\mathbf{\Omega}_t^{IRS\rightarrow BS}$).

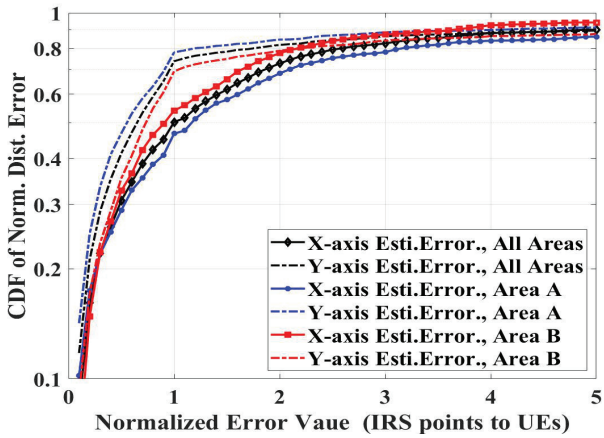

FIGURE 6. The localization performance of interference source (IRS pattern: $\mathbf{\Omega}_t^{IRS\rightarrow UEs}$).

localization accuracy at Y-axis of interference source is little higher than that of at X-axis. The reason comes from that the ULA at BS is set to be parallel to the Y-axis which makes the method have larger spatial resolution than that of X-axis. However, it also shows that the IRS patterns have little impact on the localization accuracy in both figures. These results imply that the optimal IRS pattern for maximizing is different from the pattern for the optimal interference detection/localization.

We should note that the proposed method belongs to one kind of fingerprint-based way which is sensitive to the real environments such as adding some new UEs, increasing or decreasing the obstacles. However, the proposed method can still work well if the pre-selected fingerprint samples can be fully updated when the environment of channel is changed.

For the different indoor structural scenes, the proposed method perhaps appears different localization performance. The reason is that the accuracy of the fingerprint-based localization method usually depends on the grid size during the training stage. For some indoor structural scenes, such as factory with many metal objects, the complicated wireless environments will make the variation among these known MUSIC spectrums located to these selected centers more complicated and be hard to be analyzed. Therefore, the localization accuracy could be largely reduced. However, the fingerprint-based localization method has low complexity and can coarsely detect the correct location for some simple indoor scenarios.

In addition, changing the number of BS antennas N and IRS cells M has largely impact the experimental results. When the number of BS antennas N is changed, the MUSIC spectrum will be different. Usually, the value N decides the AoA resolution. The larger value N is, the better resolution is. For the number of IRS cell M, the large value M will increase the link power between the BS and UEs via IRS device. The partial MUSIC spectrum signal which related to these links will be enlarged. Therefore, increasing the values of N and M will further improve the accuracy of interference detection and localization, and vice versa.

V. PROBABILISTIC NEURAL NETWORK-BASED PREDICTOR FOR INTERFERENCE ARRIVAL

Using the previous proposal, the interference occurrence can be detected, and the locations of interference sources can also be estimated. These results provide the possibility of that the activity data of interference source can be collected and then be predicted based on these data.

Figure 7 shows the main process of the proposed method to predict the interference arrival. We assume there are two interference sources: Interf#1 and Interf#2 which generate interference packets according to some arrival processes. We assume that the BS and two UEs are transmitting or receiving continuous signal using precoding or beamforming technique for multiple-user MIMO communication. The BS calculates the MUSIC spectrum using T_s duration of received signal and then decides whether interference exists or not. If interference occurs, BS will localize the interference source using the proposed method in previous sections. After that, the duration of T_s and next T_I duration of the localized interference source will be judged as busy (1). In a similar way, the duration of $T_s + T_I$ duration of localized interference source will be judged as idle (0) if BS judges that no interference signal transmits. After obtaining enough data of the busy/idle (1/0), the BS can learn the property of the data and utilize the learned properties to predict the interference arrival using the technology of machine learning. In this paper, we select the PNN [33] for the target of learning and prediction.

A. PROBABILISTIC NEURAL NETWORK

Based on a radial-basis function, PNN can be classified as a developed feed-forward Bayesian network. The core of PNN employs one statistical method named as Kernel density estimation which classifies the input data into different classes according to the estimated PDF of each class and

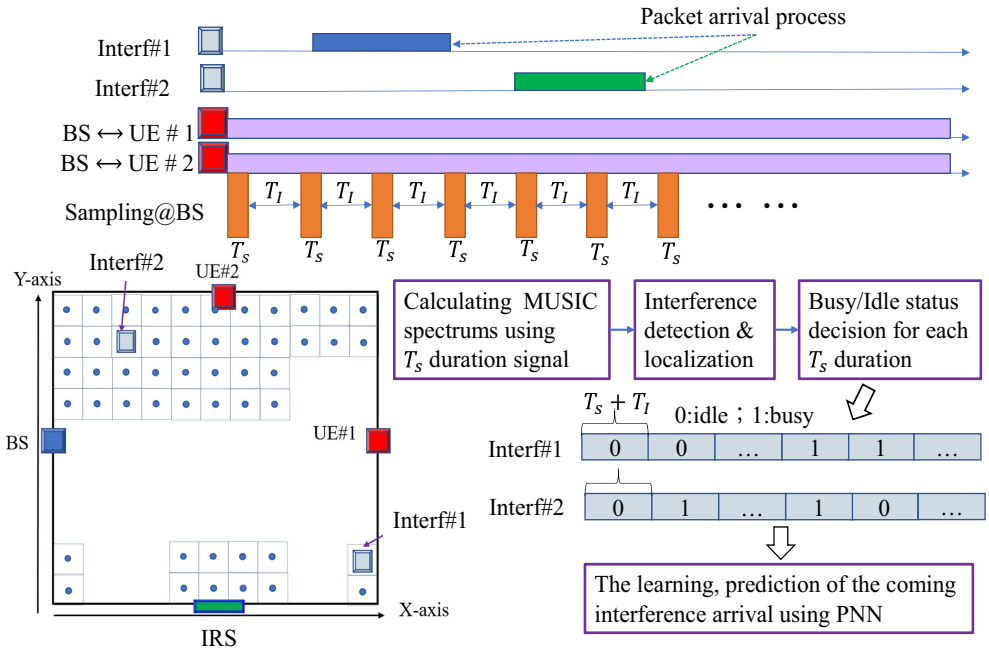

FIGURE 7. The prediction of interference arrival for mmWave IRS-MIMO system.

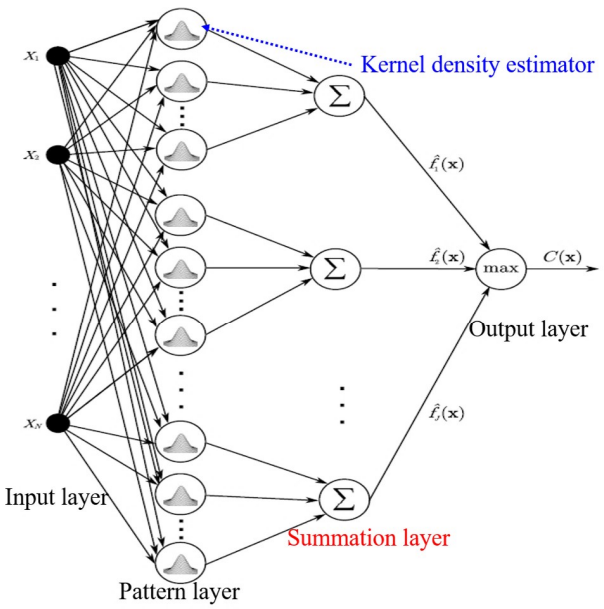

FIGURE 8. The basic model of probabilistic neural network.

optimizing the neurons weights. Fig. 8 shows the main PNN architecture which includes four major layers called as input layer, pattern layer, summation layer and final output layer, respectively. For the training stage of PNN, the data is input at the input layer and then moved to the pattern layer. Here, the Kernel density estimation is used to estimate the PDF of each class, and then classify the data into different classes. The Euclidean distance between the input data and the reference data is calculated and then multiplied by each neuron weight with a Gaussian activation function. The contribution of the ith class is then summed to get a probability value contributed from all neurons in the summation layer. Such probability can be represented as following equation,

$$P_i(x) = \frac{1}{\sigma\sqrt{2\pi}} \sum_{j=1}^{N_{E_i}} e^{-\frac{\|\mathbf{v}-\mathbf{v}_{i,j}\|^2}{2\sigma^2}}. \tag{15}$$

Here vectors $\mathbf{v}_{c,j}$, $\mathbf{v}$ are the jth training data and the sample data, respectively. N_{E_C} and σ represent the number of the ith class training vector and Gaussian spread of PNN, respectively. Therefore, the value of $||\mathbf{v} - \mathbf{v}_{i,j}||^2$ shows the squared Euclidean distance between the input data vector and the jth training data vector from the ith class. Finally, the output layer selects the class with the highest probability.

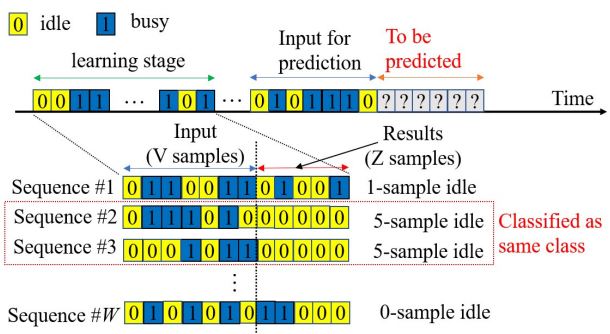

FIGURE 9. The continuous status prediction using probabilistic neural network

Using PNN, the correlation property between the input data and the output can be found. Then the new output can be predicted using the training all neurons weights. The similar

idea can be used for the continuous status busy/idle prediction [34, 35] which is shown in Fig. 9. After the interference detection and localization of each interference sources as explained in previous section, the time-series status of each interference source can be represented as 0/1 data stream which also shown and explained in Fig. 7. Therefore, the detection accuracy of interference occurrence and its location highly impacts the value of the 0/1 data stream. For example, with the perfect detection of interference occurrence and location, the 0/1 data stream can represent the correct time-series statuses of the interference and vice versa. If such time-series statuses has some correlation property, using PNN can find such relationship and predict its coming arrival correctly.

To training and testing the PNN predictor, the estimated 0/1 data stream of each interference source is used to find the correlation property. As shown in Fig. 9, the idle/busy (0/1) data stream of each interference source is divided into two parts for two different stages: learning stage and prediction stage. During learning stage, the 0/1 data is arranged as several continuous statuses or sequences which include $V+Z$ samples by shifting the data stream with an interval of one or several samples. The continuous V samples data as input data for PNN predictor is assumed to be obtained till the current time. The next continuous Z samples are assumed as the coming idle/busy data which needs to be predicted. After that, the number of continuous idle or busy samples in V data is used for classifying the different classes. For example, as shown in Fig. 9, the Sequence #2 and Sequence #3, which has 5 continuous idle samples, are classified as the same class. After that, the correlation between the input continuous V samples and each class can be learned using PNN with optimal weights for all neurons. Finally, the number of coming continuous idle samples can be predicted using the PNN with these trained weights for all neurons.

B. SIMULATION PARAMETERS OF PROBABILISTIC NEURAL NETWORK

Figure 7 also shows the simulated scenario. The parameters for interference detection and localization are the same with that in Sect. IV. Two interference sources (Interf #1, Interf #2) are located as (9.5 m, 1.5 m) and (2.5 m, 8.5 m) with 1.5 m-height antennas, respectively. For IRS pattern, we only consider the case of $\mathbf{\Omega}_t^{IRS\rightarrow UEs}$ where the IRS device is pointing to two UEs.

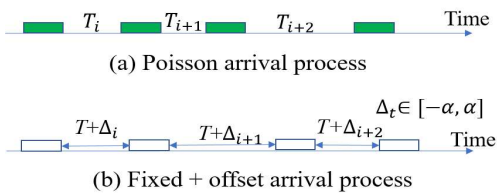

(a) Poisson arrival process

(b) Fixed + offset arrival process

FIGURE 10. The simulated interference arrival patterns.

For interference arrival pattern, we simulated two patterns: Poisson arrival and fixed transmission pattern with offset as shown in Fig. 10(a) and Fig. 10(b), respectively. For Poisson arrival, the probability of the interval T_i between two packets is distributed as $p(T_i) = \lambda e^{-\lambda T_i}$, where λ is the average arrival rate. Poisson arrival process is one of the most widely-used processes. It is usually employed for the scenario counting the occurrence of certain event that occurs with a certain rate but randomly and no correlation among the arrival time. This means that it is difficult to be predicted if interference arrival obeys the Poisson arrival process. On the contrary, for the fixed transmission pattern, we assume the interval is fixed with T. To reduce the correlation between the arrivals, some random offsets between the arrival intervals are used. The fixed transmission pattern with random offset can be assumed for some scenarios that some WLAN devices send the packets after fixed intervals but with some offset for the random backoff sensing before the start of the transmission. In this paper, we set that the random intervals are among $[T-\alpha, T+\alpha]$. Large value α can reduce the correlation among the intervals.

Table. 2 lists the PNN parameters. The duration of all packets T_P are the same set as 0.2 s. For training and prediction with PNN, the row value W is fixed as 400, and the V samples and Z samples are set with the same values. We simulate the scenario as shown in Fig. 7 for two hours which generates about 144000 busy/idle samples (50 ms/sample). In addition, according to the previous simulated results, the accuracy of interference detection for that interference signal is from one source (P_I) and two sources (P_{II}) are the same and set as 0.97. We use P_{LO} to show the probability that the interference source is correctly localized. This means that the interference sources of Interf #1 and Interf #2 are mismatched with the probability as (1-P_{LO}). From preparatory simulation, we set P_{LO} as 0.96. The high value is attributed to the stationary nature of Interf #1 and Interf #2, which are situated at a considerable distance from each other. It's important to highlight that the values of P_I, P_{II} and P_{LO} significantly influence the time-series samples, indicating busy or idle states (1/0).

TABLE 2. PNN parameters

Parameter	Value
Arrival of Poisson rate (λ)	One packet per 1.2 s.
Packet duration (T_P)	0.2 s.
Fixed interval T	1 s
MUSIC spectrum duration (T_S)	1 ms
State duration (T_I)	49 ms
Simulation duration	2 hours
Percentage of training, prediction samples	(70% ,30%), (50%, 50%)
PNN row value (W)	400
Row samples for PNN V (We set $V = R$)	200, 800
Gaussian spread value σ	0.1, 0.8

C. SIMULATION RESULTS OF INTERFERENCE ARRIVAL

We use the CCDF (complementary cumulative distribution function) of the coming continuous idle status to show the prediction results. For comparison, the real CCDF of contin-

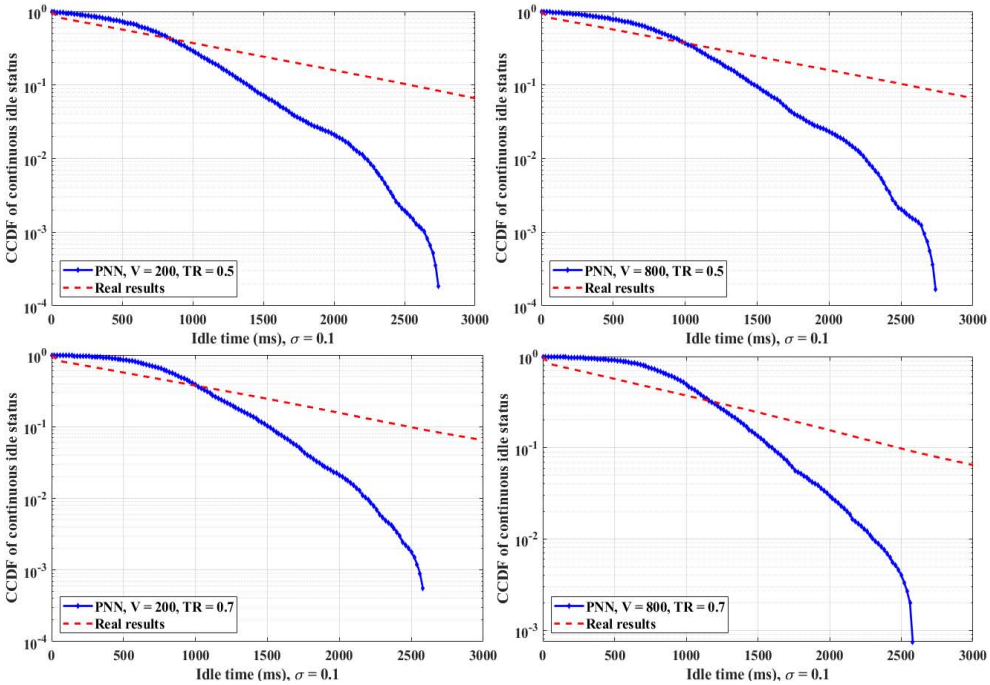

FIGURE 11. The prediction results of interference arrival (Interf#1, Poisson arrival, $\sigma = 0.1$).

uous idle status with the perfect time-series busy/idle samples of the interference source is given. Two CCDF curves will coincide each other if the prediction using PNN works perfectly.

Fig. 11(a) to Fig. 11(d) show the simulated prediction results of the interference arrival when the PNN sets $\sigma = 0.1$ with different V and ratio of training samples (TR). The interference packets are generated with a Poisson arrival process. We only show the results of Interf#1 because Interf#2 has the similar performance. As shown in all figures, the predicted results are totally inconsistent with the real results. The predicted CCDF of continuous idle duration seems to be inverse-square with the continuous idle duration which is totally different with that of the real results. The reason is that the interference arrivals occur randomly and have no correlation among the arrival time due to Poisson arrival process. Therefore, Fig. 11 shows the failure case of our proposed prediction method because Poisson arrival is independent and hard to be predicted. The PNN cannot find the correlation among the continuous idle duration during the training stage.

Fig. 12(a) to Fig. 12(d) show the simulated prediction results of the interference arrival when the PNN sets $\sigma = 0.1$ and with different V and TR when interference packets are generated as the fixed transmission pattern with offset α. The predicted CCDF results become almost consistent with the real results especially when the continuous idle duration is less than 0.8 s for both $\alpha = 0.1$ s and $\alpha = 0.2$ s. This is because the probability that the interference arrival is longer than 0.8 s is very high for the fixed transmission pattern even with offset $\alpha = 0.2$ s. However, the CCDF curve of the predicted result deviates from the real result for longer continuous duration. The larger α makes the higher level of deviation. The reason is that the error of interference detection and localization change the correct busy/idle samples to opposite values which weakens the correlation property among the time-series samples. In addition, a random offset increases the randomness of time-series samples which deteriorates the prediction accuracy.

Fig. 13(a) to Fig. 13(d) show the simulated prediction results using PNN with $\sigma = 0.8$ and with the different V and TR for the same transmission pattern in Fig. 12. The simulated results are similar to that of in Fig. 12. From both Fig. 12 and Fig. 13, changing the value V seems to have less impact on the prediction results. The reason is that it is enough to capture the correlation among time-series busy/idle samples when V is set as 200 (10 seconds) because the average packet generation time is 1.2 s. Increasing V to 800 (40 seconds) cannot dramatically change the correlation property among time-series busy/idle samples. With the similar reason, changing the ratio of training data has little influence on the prediction performance when the average packet generation time is short, and the correlation property is easily captured using only 50% of the two-hour status data.

VI. CONCLUSION

This paper has proposed a MUSIC spectrum-based low-complexity method to detect interference occurrence, localize the interference sources and then predict the interference arrival for mmWave IRS-MIMO system. The main idea is that the MUSIC spectrum can be treated as the 'signature' of the transmit/interference signals from different users at

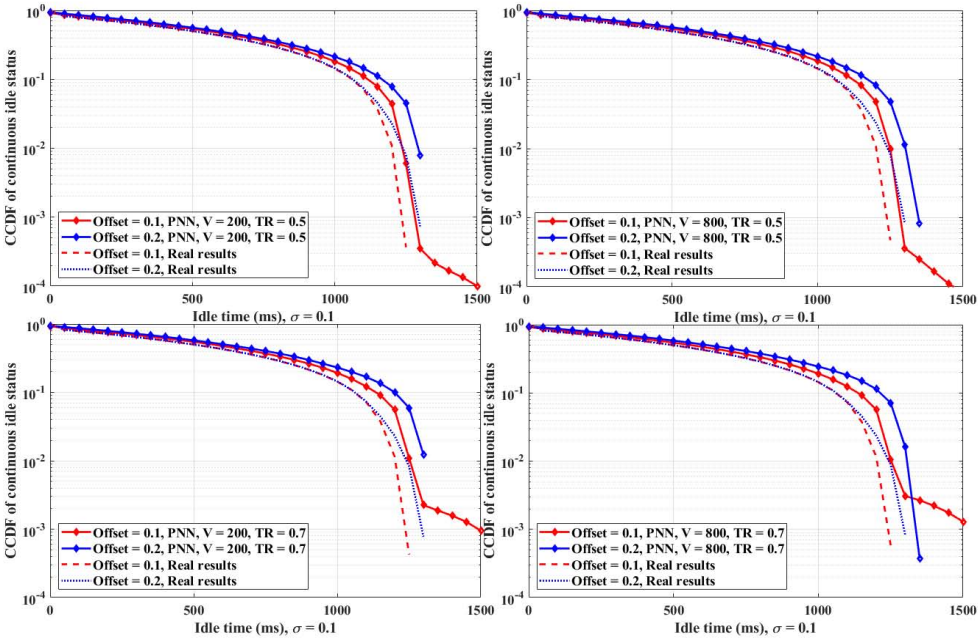

FIGURE 12. The prediction results of interference arrival (Interf#1, Fixed transmission pattern +offset (α), $\sigma = 0.1$).

different locations. This property can be used to detect the occurrence of interference and localize the their sources by only calculating the one-dimension MUSIC spectrum with less computational complexity. The simulated results confirmed that the proposed low-complexity method can provide a high accuracy of detection and the coarse information of their locations. Finally, the pattern of interference occurrence can be learned from the collected data which can be used to learn and predict the interference arrival. This paper also proposed an efficient PNN-based predictor for the prediction of interference arrival and showed its prediction accuracy. From simulated results, our proposed method can achieve the correct results with the accuracy near to 100% when the fingerprint samples is over 10. In addition, the localization error can be within 1 m with more than 65% and 43% for Y-axis and X-axis, respectively. Finally, based on the results of the interference occurrence, the proposed PNN-based predictor for the interference arrival prediction can almost capture the correct CCDF of the coming continuous idle status.

There are still many issues on this research topic. The interference detection will be difficult for moving interference sources because of the changeable AoA which generates the variable MUSIC spectrum for the same interference source. In addition, these variable MUSIC spectrums make the localization difficult using a simple fingerprint-based method. On the other hand, the interference arrival pattern highly relies on the accuracy of the detection and localization. How to find the correct pattern and realize good prediction accuracy becomes a sizeable issue when considering moving interference sources with a large path loss on the transmission link. Some solutions perhaps depend on the joint optimization of the MIMO system and IRS devices. In addition, this paper is less consideration for usage of IRS. The main usage of IRS in this research is to increase the link power by making the IRS point to the BS or UEs. It should bring new and interesting technical challenges if the target of introducing IRS for the detection of interference occurrence or localization the interference sources. Finally, the results are all from simulation but not from real experimental results. These research topics will be our future research directions.

REFERENCES

[1] B. Zong, C. Fan, X. Wang, et al., "6G Technologies: key drivers, core requirements, system architectures, and enabling technologies," *IEEE Veh. Technol. Mag.*, vol. 14, no. 3, pp. 18–27, Sept. 2019, doi: 10.1109/MVT.2019.2921398.

[2] Y. Jiang et al., "Toward URLLC: A full duplex relay system with self-interference utilization or cancellation," *IEEE Wirel. Communi.*, vol. 28, no. 1, pp. 74–81, Feb. 2021, doi: 10.1109/MWC.001.2000238.

[3] S. Zhang, J. Liu et al., "Envisioning device-to-device communications in 6G," *IEEE Netw.*, vol. 34, no. 3, pp. 86–91, May/June 2020, doi: 10.1109/MNET.001.1900652.

[4] F. Liu et al., "Seventy years of radar and communications: The road from separation to integration," *IEEE Sig. Proc. Mag.*, vol. 40, no. 5, pp. 106–121, July 2023, doi: 10.1109/MSP.2023.3272881.

[5] G. C. Alexandropoulos, N. Shlezinger et al., "Hybrid reconfigurable intelligent metasurfaces: Enabling simultaneous tunable reflections and sensing for 6G wireless communications," *IEEE Veh. Technol. Mag.*, vol. 19, no. 1, pp. 75–84, Mar. 2024, doi: 10.1109/MVT.2023.3332580.

[6] M. Alsabah et al., "6G Wireless Communications Networks: A Comprehensive Survey," *IEEE Access*, vol. 9, pp. 148191–148243, 2021.

[7] E. Bjornson, L. Van der Perre, et al., "Massive MIMO in sub-6 GHz and mmWave: physical, practical, and use-Case differences," *IEEE Wirel. Communi.*, vol. 26, no. 2, pp. 100–108, April 2019.

[8] M. M. Azari et al., "Evolution of non-terrestrial networks from 5G to 6G: a survey," *IEEE Communi. Sur. & Tut.*, vol. 24, no. 4, pp. 2633–2672, Fourthquarter 2022.

[9] E. C. Strinati et al., "Reconfigurable,intelligent, and sustainable wireless environments for 6G smart connectivity," *IEEE Communi. Mag.*, vol. 59, no. 10, pp. 99–105, Oct. 2021.

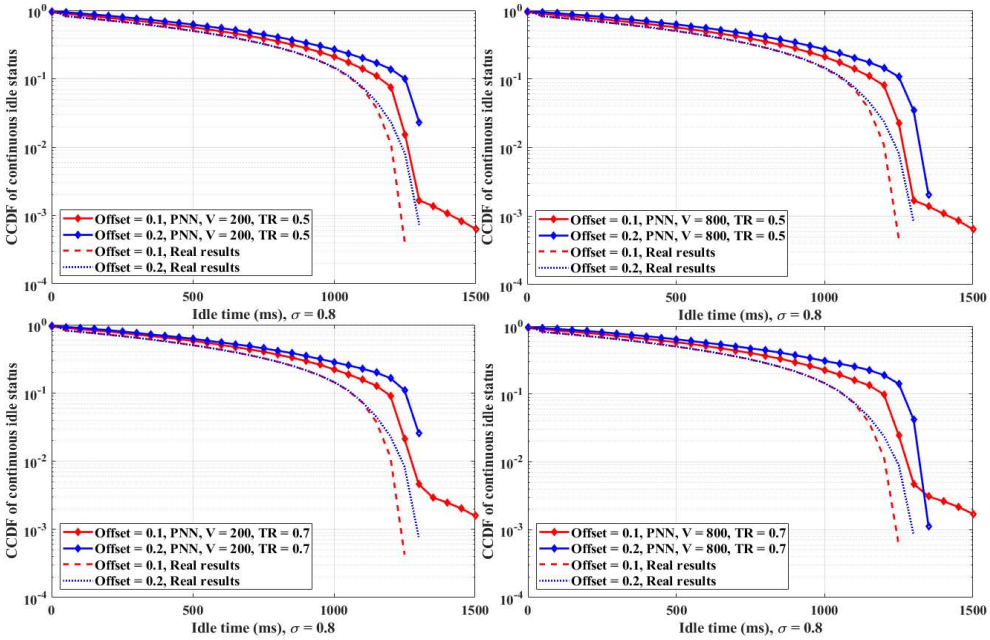

FIGURE 13. The prediction results of interference arrival (Interf#1, Fixed transmission pattern +offset (α) , $\sigma = 0.8$).

[10] D. Wei, S. Zhang, et al., "Research on anti-jamming technology of chaotic composite short range detection system based on underdetermined signal separation and spectral analysis", *IEEE Access*, vol. 7, pp. 42298–42308, 2019.

[11] Y. Hou, J. Webber, et al., "Modeling and predictability analysis on channel spectrum status over heavy wireless LAN traffic environment", *IEEE Access*, vol. 9, pp. 85795–85812, 2021.

[12] S. Grimaldi, et al., "Real-time interference identification via supervised learning: embedding coexistence awareness in IoT devices," *IEEE Access*, vol. 7, pp. 835–850, 2019.

[13] K. Nakanishi, H. Mori, et al., "A novel signal detection method for interference from inverter microwave ovens in WLAN systems," Proc. 2017 IEEE Global Communi. Conf. (GLOBECOM 2017), pp. 1–6, 2017.

[14] K. Nakanishi, H. Mori, et al., "Signal detection method for interference from inverter microwave ovens in WLAN systems," *IEEE Trans. Cog. Communi. and Netw.*, vol. 4, no. 2, pp. 368–378, June 2018. doi: 10.1109/TCCN.2018.2838677.

[15] M. Mehrnoush and S. Roy, "Coexistence of WLAN network with radar: detection and interference mitigation," *IEEE Trans. Cog. Communi. and Netw.*, vol. 3, no. 4, pp. 655–667, Dec. 2017. doi: 10.1109/TCCN.2017.2762663.

[16] J. Webber, K. Yano, et al., "WLAN interference identification using a convolutional neural network for factory environments," *J. of Communi.*, vol. 16, no. 7, pp. 276–283, July 2021. doi: 10.12720/jcm.16.7.276-283

[17] F. Zafari, A. Gkelias and K. K. Leung, "A survey of indoor localization systems and technologies," *IEEE Communi. Sur. & Tut.*, vol. 21, no. 3, pp. 2568-2599, thirdquarter. 2019.

[18] X. Wang, L. Gao, S. Mao and S. Pandey, "CSI-based fingerprinting for indoor localization: a deep learning approach," *IEEE Trans. on Vehi. Techn.*, vol. 66, no. 1, pp. 763-776, Jan. 2017.

[19] A. Nessa, B. Adhikari, F. Hussain and X. N. Fernando, "A survey of machine learning for indoor positioning," *IEEE Access*, vol. 8, pp. 214945–214965, 2020.

[20] C. Pan, J. Zhou, K. Zhi et al., "An overview of signal processing techniques for RIS/IRS-aided wireless systems," *IEEE J. Sel. Top. Signal Process*, vol. 16, no. 5, pp. 883–917, Aug. 2022,

[21] Y. Pan, C. Pan, S. Jin and J. Wang, "RIS-aided near-field localization and channel estimation for the terahertz system," *IEEE J. Sel. Top. Signal Process*, vol. 17, no. 4, pp. 878–892, July 2023.

[22] Hayes, Monson H., Statistical Digital Signal Processing and Modeling, John Wiley & Sons, Inc., 1996.

[23] M. Di Renzo and S. Tretyakov, "Reconfigurable intelligent surfaces [Scanning the Issue]," *Proc. of the IEEE*, vol. 110, no. 9, pp. 1159–1163, Sept. 2022. doi: 10.1109/JPROC.2022.3194589.

[24] B. Li, S. Wang, et al., "Fast randomized-MUSIC for mm-Wave massive MIMO radars," *IEEE Trans. on Vehi. Techn.*, vol. 70, no. 2, pp. 1952–1956, Feb. 2021. doi: 10.1109/TVT.2021.3051266.

[25] E. Bjornson and L. Sanguinetti, "Power scaling laws and near-Field behaviors of massive MIMO and intelligent reflecting surfaces," *IEEE Open J. of the Communi. Soc.*, vol. 1, pp. 1306–1324, 2020. doi: 10.1109/OJCOMS.2020.3020925.

[26] Z. Abu-Shaban, K. Keykhosravi,et al., "Near-field localization with a reconfigurable intelligent surface acting as lens," in Proc. 2021 IEEE Int. Conf. on Communi. (ICC 2021), Montreal, QC, Canada, 2021, pp. 1–6, doi: 10.1109/ICC42927.2021.9500663.

[27] K. T. Selvan and R. Janaswamy, "Fraunhofer and Fresnel distances: Unified derivation for aperture antennas," *IEEE Antennas and Propagation Magazine*, vol. 59, no. 4, pp. 12–15, Aug. 2017, doi: 10.1109/MAP.2017.2706648.

[28] T. Zhang, P. Teng, et al., "Quasi-closed-form algorithms for spherical Angle-of-Arrival source localization," *IEEE Trans. on Sig. Proc.*, vol. 72, pp. 432–448, 2024, doi: 10.1109/TSP.2023.3340879.

[29] T. Wu et al.,"Joint angle estimation error analysis and 3-D positioning algorithm design for mmWave positioning system," *IEEE Internet Things J.*, vol. 11, no. 2, pp. 2181–2197, Jan. 2024, doi: 10.1109/JIOT.2023.3292431.

[30] B. Li, S. Wang, et al., "Fast randomized-MUSIC for mm-Wave massive MIMO radars," *IEEE Trans. on Veh. Techn.*, vol. 70, no. 2, pp. 1952–1956, Feb. 2021. doi: 10.1109/TVT.2021.3051266.

[31] A. E. -R. Nada and A. M. H. Mehana, "A comparative study of PMI/RI selection schemes for LTE/LTEA systems," *IEEE Trans. on Veh. Techn.*, vol. 67, no. 2, pp. 1444–1453, Feb. 2018, doi: 10.1109/TVT.2017.2759205.

[32] Study on channel model for frequencies from 0.5 to 100 GHz, 3GPP TR 38.901 version 16.1.0 Release 16, Dec. 2019.

[33] Donald F. Specht, "Probabilistic neural networks," *Neural Netw.*, vol. 3, no. 1, pp. 109–118, Mar. 1999, doi: 10.1016/0893-6080(90)90049.

[34] J. Webber, A. Mehbodniya, et al., "Study on idle slot availability prediction for WLAN using a probabilistic neural network," in Proc. 2017 23rd Asia-Pacific Conf. on Communi. (APCC 2017), Perth, WA, Australia, 2017, pp. 1–6, doi: 10.23919/APCC.2017.8304030.

[35] K. Yano, N. Egashira, et al., "Achievable throughput of multiband wireless LAN using simultaneous Transmission over multiple primary channels assisted by idle length prediction based on PNN," in Proc. 2019 Int. Conf.

on Arti. Intelli. in Info. and Communi. (ICAIIC 2019), Okinawa, Japan, 2019, pp. 22–27, doi: 10.1109/ICAIIC.2019.8668975.

YAFEI HOU [M-07, SM-16] received the dual Ph.D. degree from the Kochi University of Technology, Japan, and Fudan University, China, in 2007. From 2007 to 2010, he was a Postdoctoral Research Fellow with Ryukoku University, Japan. Then he was a Research Scientist at ATR Institute International, Japan till March 2014, and a Guest Researcher of ATR till 2024. He was an Assistant Professor with Nara Institute of Science and Technology from 2014 to 2017. He is currently an Associate Professor with Okayama University, Japan. He is a Senior Member of IEICE and received the Best Tutorial Paper Award in 2017, Best Paper Award, in 2016 and 2020 of IEICE Communications Society. His research interests include wireless communication systems, and signal processing. Dr. Hou serves as an Associate Editor for IEEE Access.

KAZUTO YANO [S-01, M-06] received his B.E. degree, and the M.S. and Ph.D. degrees from Kyoto University in 2000, 2002, and 2005, respectively. He was a research fellow at the Japan Society for the Promotion of Science (JSPS) from 2004 to 2006. In 2006, he joined the Advanced Telecommunications Research Institute International (ATR). Currently, he is the head of Department of Wireless Communication Systems at Wave Engineering Laboratories, ATR. His research interests include space-time signal processing for interference suppression, MIMO transmission, and PHY/MAC cross-layer design of wireless communication systems for ISM bands. He received IEICE (the Institute of Electronics, Information and Communication Engineers) Communications Society Best Tutorial Paper Award in 2017, and ICAIIC 2019 Excellent Paper Award in 2019. He is a senior member of IEICE. He serves Vice Chair of IEEE 802.19 Task Group 3a (TG3a).

NORISATO SUGA received the B.E., M.E., and Ph.D. degrees from Tokyo University of Science, Tokyo, Japan, in 2011, 2013, and 2016, respectively. From 2016 to 2019, he was a researcher at the ATR Institute International (ATR). From 2019 to 2022, he was an assistant professor at the Tokyo University of Science. Since 2022, he has been an assistant professor at the Faculty of Information and Communications Engineering, Shibaura Institute of Technology, Japan. His current research interests include digital signal processing and the quality prediction of wireless communication systems.

JULIAN WEBBER [M-97, SM-16] received the M.Eng. degree from the University of Bristol, UK in 1996. He worked at Texas Instruments, Europe from Sep. 1996 to Oct. 1998 and received the Ph.D. degree from University of Bristol in 2004. He was a Research Fellow at Bristol University from Nov. 2001 to Aug. 2007 and at Hokkaido University, Japan from Sep. 2007 to Mar. 2012. He was a research scientist at Wave Engineering Laboratories, ATR Institute International, Japan from Apr. 2012 to Mar. 2018. He became an Assistant Professor at Osaka University from Apr. 2018 and a guest research scientist at ATR. Currently, he is Associate Professor at Kuwait College of Science and Technology, Doha Area, Kuwait. His research interests include signal processing, wireless communication systems design and implementation. He is a senior member of the IEEE and member of the IEICE.

SATOSHI DENNO received the M.E. and Ph.D degrees from Kyoto University, Japan in 1988 and 2000, respectively. He joined NTT radio communications systems labs, Japan, in 1988. In 1997, he was seconded to ATR adaptive communications research laboratories, Japan. From 2000 to 2002, he worked for NTT DoCoMo, Japan then moved to DoCoMo communications laboratories Europe GmbH, Germany from 2002. From 2004 to 2011, he was an associate professor at Kyoto University. He is a full professor at Okayama University, Japan Since 2011. From the beginning of his research career, he has been engaged in the R&D of digital mobile radio communications, in particular, in channel equalization, array signal processing, Space time codes, spatial multiplexing, and multimode reception. He received the Excellent Paper Award from the IEICE in 1995 and IEICE Communications Society Best Paper Awards in 2020.

TOSHIKAZU SAKANO received the B.E., M.E., and Ph.D. degrees from Tohoku University, Japan, in 1985, 1987, and 1998, respectively. He joined Nippon Telegraph and Telephone Corporation (NTT) Network Innovation Laboratories, Japan in 1987, where he has been active in several R&D fields, including optical signal processing, super-high-definition imaging systems, photonic network architectures, and large-capacity optical transmission systems. After March 2011, he has engaged in the R&D of resilient information communication technology. Since January 2015, he was the Director of the Business Development Office with ATR Institute International, Kyoto, Japan. Currently, he is the director of ATR Wave Engineering Laboratories. Dr. Sakano is a Senior Member of The Optical Society and IEICE. He was a recipient of the Young Engineer Award from IEICE in 1995.